Research Square

Preprints are preliminary reports that have not undergone peer review.
They should not be considered conclusive, used to inform clinical practice,
or referenced by the media as validated information.

Preparation and electrochemical behavior of amorphous Co-Mo coating with high content of Mo

Ya Tian
Beijing University of Technology
Liwen Ma
Beijing University of Technology
Xiaoli Xi (xixiaoli@bjut.edu.cn)
Beijing University of Technology
Zuoren Nie
Beijing University of Technology

Article

Keywords: Electrodeposition, Amorphous Co-Mo coating, Microhardness, Electrochemical mechanism

Posted Date: March 24th, 2022

DOI: https://doi.org/10.21203/rs.3.rs-1437984/v1

License: This work is licensed under a Creative Commons Attribution 4.0 International License.
Read Full License

Abstract

At present, alloy materials have been widely used as wear-resistant coatings due to good mechanical properties. In this paper, electrodeposition was used to prepare the Co-Mo coating. The electrochemical behavior of the deposition of alloy and the phase composition, morphology, composition and property of the coating have been studied. The study of process parameters found that when the concentration of Na_2Mo_4 is 0.05mol/L, the concentration of $C_6H_5Na_3O_7$ is 0.15mol/L, the pH of the solution is 7, and the temperature is 50℃, the content of Mo in Co-Mo coating is 39.56%, and the microhardness reaches the maximum value of 503HV. The study of electrochemical behavior found that when the concentration of Na_2Mo_4 is 0.05mol/L, the concentration of $C_6H_5Na_3O_7$ is 0.15mol/L, the pH of the solution is 7 and the temperature is 50℃, the most positive deposition potential, maximum exchange current density and minimum charge transfer impedance were obtained, which explained why the best performance coating can be obtained under this condition.

1. Introduction

Alloy materials have been widely used due to their good mechanical properties. The traditional method of preparing alloy materials is mainly powder metallurgy, but the electrodeposition can be used to prepare alloy coatings on the substrate in a salt solution to improve the property of the substrate materials.

Currently, the more widely used alloy coatings mainly include Ni-Co alloy, Ni-W alloy [1, 2], Co-W alloy [3–5], Ni-Mo alloy [6–9], Co-Mo alloy [10–12], Ni-Co-Mo alloy [13] and other iron group element alloys[14–17]. Among them, the content of W [18, 19] and Mo [20, 21] is critical to the performance of the coating. Due to its good mechanical properties and catalytic hydrogen evolution performance, the molybdenum-containing coating have been used as wear-resistant coating and catalytic hydrogen evolution material in the field of metal protection and water electrolysis. N. P. Wasekar et al. [8] prepared a Ni-Mo alloy coating and found that the increase in molybdenum content improved the microhardness, wear resistance and corrosion resistance of the coating. C. Y. Lee et al.[21] studied the corrosion behavior of Ni-Mo coating in NaCl solution, found that the corrosion film was not passivated under high overpotential, and the synergistic effect of wear and corrosion on the weight loss of this Ni-Mo alloy coating was less obvious than that of other Ni alloy coatings. Some researchers have studied the principle of electrodeposition and electrochemical behavior of molybdenum-containing alloys. Elvira Go´mezet al.[11] used voltammetry to study the influence of process parameters on co-deposition of cobalt and molybdenum. At present, most of the Co-Mo coatings show crystalline structure, while the amorphous Co-Mo coating with high Mo content possess better property. And the relationship between the electrochemical behavior of the alloy and the structure, composition, morphology and property of the coating has not been deeply studied. Therefore, in this paper, the amorphous Co-Mo coating with high Mo content was prepared by optimization of process electrodeposition and the effect of different process parameters on the electrochemical behavior, structure, morphology, composition and property of coating was studied.

2. Experimental

2.1 Coating preparation

The Co-Mo coating was prepared by electrodeposition in a citrate bath. The composition of the bath and process parameters are shown in Table 1. All reagents are analytically pure, using anionic surfactant $C_{12}H_{25}SO_4N$ as the dispersant. Use dilute sulfuric acid and sodium hydroxide solution to adjust the pH of the solution. Electrodeposition was carried out in a 200 mL beaker. The anode of the double graphite plate was inserted into the electroplating solution in parallel, and the copper sheet was used as the cathode, suspended in the middle of the double graphite plate. The substrate is pretreated before deposition, using 600#, 800#, 2000# sandpaper for mechanical polishing, and 6μm, 3μm polishing liquid for polishing. Then use sodium hydroxide for chemical degreasing, dilute sulfuric acid for activation, and use alcohol to clean in an ultrasonic cleaning machine, finally wash with distilled water and dry.

Table 1
Bath composition and electroplating parameters for deposition of coatings.

Bath composition		**Electrodeposition conditions**	
$CoSO_4$	0.1mol/L	pH	6 ~ 9
Na_2MoO_4	0.05 ~ 0.15mol/L	Temperature	40 ~ 60℃
$Na_3C_6H_5O_7$	0.1 ~ 0.3mol/L	Current density	$1A{\cdot}dm^{-2}$
$C_{12}H_{25}SO_4Na$	1g/L	Deposition time	2h

The current efficiency is calculated according to Eq. (1):

$$\eta = \left(\frac{\{\rm M\} \times f_{Co}}{C_{Co} \times I \times t} + \frac{\{\rm M\} \times f_{Mo}}{C_{Mo} \times I \times t} \right) \times 100\%$$

1

Where, M is the quality of the obtained alloy coating, f is the mass fraction of each metal in the coating, C is the electrochemical equivalent of each metal in the coating, I is the current intensity, and t is the electrodeposition time.

2.2 Coating characterization

The surface morphology of the coating was characterized by scanning electron microscope (SEM-2100) and the composition of the coating was studied using an energy dispersive X-ray spectrometer (EDS) coupled with SEM. The structure was analyzed by X-ray diffraction method (XRD-7000) under copper Kα1 radiation, and the measurement was carried out in the range of 2θ from 10° to 90°.

2.3 Coating performance test

The Microhardness of the coating was examined by HXD-100TMC/LCD micro-hardness tester. The applied force is 0.05mm/s, the applied load is 100g, and the holding time is 10s. Each sample was tested for the hardness value of 10 points and find the average.

2.4 Electrochemical behavior test

A three-electrode system was used for electrochemical testing in a 200ml beaker containing electroplating solution. The glassy carbon electrode and copper electrode were used as the working electrode, the platinum electrode was used as the auxiliary electrode, and the saturated calomel electrode was used as the reference electrode. The cyclic voltammetry(CV) was performed at a scan rate of 50mV/s within the potential range of -1.2V~-0.5V, the linear scan voltammetry(LSV) was performed at a scan rate of 50mV/s within the potential range of -1.2V ~ 0V, and the electrochemical impedance spectroscopy(EIS) was performed in the range of 0.1 Hz-10k Hz with the potential of -1.2V.

3 Results And Discussion

3.1 The structure, composition, morphology and property of Co-Mo coating

3.1.1 Effect of the concentration of Na_2MoO_4

The XRD spectra of the Co-Mo coatings at different concentrations of Na_2MoO_4 are shown in Fig. 1(a). The XRD spectra of the coatings with different concentrations of Na_2MoO_4 showed a broad diffraction peak around $2\theta = 43°$, indicating that the Co-Mo coating is an alloy with an amorphous structure. The XRD spectra of the coatings prepared with the concentration of Na_2MoO_4 at 0.075 mol/L, 0.1 mol/L, 0.125 mol/L and 0.15 mol/L show the diffraction peak of copper at $2\theta = 50°$ and $2\theta = 74°$, and a less obvious broadened diffraction peak is shown near $2\theta = 43°$. Combined with electrochemical test of different concentrations of Na_2MoO_4, it was shown that as the concentration of Na_2MoO_4 increases, the deposition of alloy becomes more and more difficult, so the coating becomes thin, causing X-rays to hit the copper substrate.

Figure 1(b) shows the influence of the concentration of Na_2MoO_4 in the plating solution on the composition and current efficiency of the Co-Mo coatings. As the concentration of Na_2MoO_4 increases, the mass fraction of molybdenum in the coating shows a trend of first decreasing and then increasing. When the concentration of Na_2MoO_4 in the plating solution is 0.05mol/L, the content of molybdenum reaches the maximum value of 37.25%. It is reported that the greater the concentration of Na_2MoO_4 in the plating solution in a certain range, the higher the content of molybdenum in the coating. However, the electrochemical test results of different sodium molybdate concentrations shows that as the

concentration of Na_2MoO_4 increases, the exchange current density i_0 decreases, the charge transfer resistance *Rct* increases, which is conducive to the separate deposition of cobalt and hinders the co-deposition of cobalt and molybdenum. At the same time, as the concentration of Na_2MoO_4 increases, the thickness of the coating becomes thinner, resulting in the determination of the mass fraction of coating components, the copper matrix also occupies a certain mass fraction.

As the concentration of Na_2MoO_4 in the plating solution increases, the current efficiency decreases. This is because as the concentration of Na_2MoO_4 increases, the deposition of alloy becomes difficult and the coating quality decreases. According to the Eq. (2 − 1), the current efficiency decreases.

The surface morphology of the Co-Mo coating under different concentrations of Na_2MoO_4 is shown in Fig. 2. When the concentration of Na_2MoO_4 is 0.05 mol/L, the Co-Mo coating has the characteristics of the surface morphology of nodular shape, the surface is flat and smooth, and the crystal grains are small and uniform. This is due to the higher content of molybdenum in the coating. When the concentration of Na_2MoO_4 increases, the surface quality of the coating is reduced, the surface becomes uneven, and the crystal grains become coarse.

Figure 3 shows the comparison of the microhardness of the Co-Mo coating with different concentrations of Na_2MoO_4. As the concentration of Na_2MoO_4 in the plating solution increases, the microhardness of the Co-Mo coating is reduced. When the concentration of Na_2MoO_4 is 0.075 mol/L, 0.1 mol/L, 0.125 mol/L and 0.15 mol/L, The microhardness of Co-Mo coating are 289.486HV、268.462 HV、240.938 HV、207.722 HV. When the concentration of Na_2MoO_4 is 0.05 mol/L, the microhardness of the Co-Mo coating reaches the maximum value of 331HV.

From the perspective of the structure of coating, the coating is an amorphous alloy, indicating that molybdenum enters the cobalt lattice, causing lattice distortion, which hinders the movement of dislocations and improves the microhardness of the coating. Therefore, the higher the content of molybdenum in the coating, the higher the microhardness. Moreover, as the concentration of Na_2MoO_4 increases, the thickness of the coating decreases. During the microhardness test, the diamond probe may release the copper matrix. The microhardness of copper is about 200HV, which makes the microhardness of the coating low.

3.1.2 Effect of the concentration of $C_6H_5Na_3O_7$

The XRD spectra of the Co-Mo coatings at different concentrations of $C_6H_5Na_3O_7$ are shown in Fig. 4(a). The XRD spectra of the coatings with different concentrations of $C_6H_5Na_3O_7$ showed a broad diffraction peak around 2θ = 43°. The XRD spectra of the coatings prepared with the concentration of $C_6H_5Na_3O_7$ at 0.2 mol/L, 0.25 mol/L and 0.3 mol/L show the diffraction peak of copper at 2θ = 50° and 2θ = 74°, and a less obvious broadened diffraction peak is shown near 2θ = 43°. Combined with electrochemical test of

different s concentrations of $C_6H_5Na_3O_7$, it was shown that when the concentration of $C_6H_5Na_3O_7$ is too high, the deposition of alloy becomes difficult, so the coating becomes thin, causing X-rays to hit the copper substrate.

Figure 4(b) shows the influence of the concentration of $C_6H_5Na_3O_7$ in the plating solution on the composition and current efficiency of the Co-Mo coatings. As the concentration of $C_6H_5Na_3O_7$ increases, the mass fraction of molybdenum in the coating shows a trend of first increasing and then decreasing. When the concentration of $C_6H_5Na_3O_7$ in the plating solution is 0.15mol/L, the content of molybdenum reaches the maximum value of 37.25%. The deposition of molybdenum mainly depends on the formation of cobalt-molybdenum complex ions. Combined with the electrochemical test results, when the concentration of $C_6H_5Na_3O_7$ in the solution is too low, the optimal concentration for forming complex ions cannot be achieved, which is not conducive to the deposition of molybdenum. When the concentration of $C_6H_5Na_3O_7$ increases to 0.15 mol/L, the exchange current density reaches the maximum value and the charge transfer resistance reaches the minimum value. At this time, the deposition of alloy is easier, and the content of molybdenum in the coating reaches the maximum value. With the further increase of the $C_6H_5Na_3O_7$ concentration, excessive ions hinder the movement of complex ions to the cathode, the exchange current density begins to decrease, the charge transfer resistance begins to increase, alloy deposition becomes difficult, and the molybdenum content in the coating decreases.

As the concentration of $C_6H_5Na_3O_7$ in the plating solution increases, the current efficiency increases first and then decreases. This is because as the concentration of $C_6H_5Na_3O_7$ increases, the deposition of alloy becomes easy and the coating quality increases, according to the Eq. (2 – 1), the current efficiency increases. However, as the concentration of $C_6H_5Na_3O_7$ further increases, the deposition of the alloy is hindered, and the quality of the coating decreases. According to the Eq. (2 – 1), the current efficiency decreases.

The surface morphology of the Co-Mo coating under different concentrations of $C_6H_5Na_3O_7$ is shown in Fig. 5. When the concentration of $C_6H_5Na_3O_7$ is 0.1 mol/L, the Co-Mo coating has the characteristics of the surface morphology of irregular polygonal flakes. When the concentration of $C_6H_5Na_3O_7$ is 0.15 mol/L, the surface is flat and smooth, and the crystal grains are small and uniform. This is due to the higher content of molybdenum in the coating. When the concentration of $C_6H_5Na_3O_7$ continue to increase, the surface becomes uneven, and the crystal grains become coarse.

Figure 6 shows the comparison of the microhardness of the Co-Mo coating with different concentrations of $C_6H_5Na_3O_7$. As the concentration of Na_2MoO_4 in the plating solution increases, the microhardness of the Co-Mo coating increases first and then decreases. When the concentration of $C_6H_5Na_3O_7$ is 0.1mol/L, 0.2 mol/L, 0.25mol/L and 0.3mol/L, the microhardness of Co-Mo coating is 314HV, 284.4HV, 270.2HV and 251.6HV, respectively. When the concentration of $C_6H_5Na_3O_7$ is 0.15 mol/L, the microhardness of the Co-Mo coating reaches the maximum value of 331HV. As the concentration of $C_6H_5Na_3O_7$ increases, the content of molybdenum in the coating first increases and then decreases, and the degree of lattice

distortion caused first increases and then decreases. Therefore, the microhardness of the coating first increases and then decreases.

3.1.3 Effect of the pH value

The XRD spectra of the Co-Mo coatings under different pH are shown in Fig. 7(a). The XRD spectra of the coatings under different temperature showed a broad diffraction peak around 2θ = 43°. The XRD spectra of the coatings prepared with the pH at 6 and 9 show the diffraction peak of copper at 2θ = 50° and 2θ = 74°, and a less obvious broadened diffraction peak is shown near 2θ = 43°. Combined with electrochemical test of different temperature, it was shown that as the pH rises, the deposition of alloys becomes more difficult, but when the pH is 6, the alloy deposition rate is too fast, and the hydrogen evolution reaction is violent due to the high concentration of H^+ in the electroplating solution, causing the coating surface to fall off causing the coating surface to peel off, which makes the coating thinner causing X-rays to hit the copper substrate.

Figure 7(b) shows the influence of the pH on the composition and current efficiency of the Co-Mo coatings. As the pH increases, the mass fraction of molybdenum in the coating shows a trend of decreasing. When the pH is 6, the content of molybdenum reaches the maximum value of 38.98%. Combined with the electrochemical test results, as the pH increases, the exchange current density decreases, and the charge transfer resistance increases, which makes the deposition of alloy more difficult, so the content of molybdenum in the coating decreases.

As the pH increases, the current efficiency increases first and then decreases. When the pH is 7, the current efficiency reaches the maximum value. The low current efficiency is due to the high content of molybdenum. The deposition of MoO_4^{2-} is not a one-step reduction to Mo. The first stage is the reduction of MoO_4^{2-} to low-valent molybdenum oxides, such as MoO_2, under the action of $CoCit^-$. At this stage, there is a hydrogen evolution reaction, so this leads to a decrease in current efficiency[22]. Therefore, when the pH is 6, the current efficiency is low. However, when the pH is too high, the deposition quality is reduced, resulting in a decrease in current efficiency.

The surface morphology of the Co-Mo coating under different pH is shown in Fig. 8. As the pH rises, the surface of the coating becomes smoother and the crystal grains are smaller. When the pH is 8 and 9, the Co-Mo coating has the characteristics of the surface morphology of irregular polygonal flakes. This is due to the lower content of molybdenum in the coating.

Figure 9 shows the comparison of the microhardness of the Co-Mo coating under different pH. As the pH increases, the microhardness of the Co-Mo coating increases first and then decreases. When the pH is 6, 8 and 9, the microhardness of Co-Mo coating are 276 HV、269.46 HV、245.93 HV. When the pH is 7, the microhardness of the Co-Mo coating reaches the maximum value of 331HV. The higher the content of molybdenum in the coating, the greater the hardness of the coating. When the pH is 6, although the

content of molybdenum in the coating is high, the surface of the coating falls off, causing the diamond probe to contact the copper substrate during the microhardness test, which makes the microhardness of the coating lower.

3.1.4 Effect of the temperature

The XRD spectra of the Co-Mo coatings under different temperature are shown in Fig. 10(a). The XRD spectra of the coatings under different temperature showed a broad diffraction peak around 2θ = 43°. The XRD spectra of the coatings prepared with the temperature at 40℃, 55℃and 60℃ show the diffraction peak of copper at 2θ = 50° and 2θ = 74°, and a less obvious broadened diffraction peak is shown near 2θ = 43°. Combined with electrochemical test of different temperature, it was shown that as the temperature rises, the deposition of the alloy becomes easier, but when the temperature is too high, the deposition rate is too fast, causing the coating surface to peel off, which makes the coating thinner causing X-rays to hit the copper substrate.

Figure 10(b) shows the influence of the temperature on the composition and current efficiency of the Co-Mo coatings. As the temperature increases, the mass fraction of molybdenum in the coating shows a trend of first increasing and then decreasing. When the temperature is 50℃, the content of molybdenum reaches the maximum value of 39.56%. The deposition of molybdenum mainly depends on the formation of cobalt-molybdenum complex ions. Combined with the electrochemical test results, as the temperature increases, the migration rate of complex ions to the cathode increases, the exchange current density increases, and the charge transfer resistance decreases, which makes the deposition of alloy easier, so the content of molybdenum in the coating increases. However, when the temperature is too high, it will affect the stability of the complex ions, which is not conducive to the deposition of molybdenum, resulting in a decrease in the content of molybdenum in the coating.

As the temperature increases, the current efficiency increases first and then decreases. When the temperature is 50℃, the current efficiency reaches the maximum value of 63%. This is because as the temperature increases, the deposition of alloy becomes easy and the coating quality increases, according to the Eq. (1), the current efficiency increases. However, as the temperature further increases, the deposition rate is too fast, causing the coating surface to fall off and reduce the quality, according to the Eq. (2 − 1), the current efficiency decreases.

The surface morphology of the Co-Mo coating under different temperature is shown in Fig. 11. When the temperature is 40℃, the Co-Mo coating has the characteristics of the surface morphology of irregular polygonal flakes. As the temperature rises, the surface of the coating becomes smoother and the crystal grains are smaller. This is due to the higher content of molybdenum in the coating. When the temperature is too high, the surface becomes uneven, and the crystal grains become coarse.

Figure 12 shows the comparison of the microhardness of the Co-Mo coating under different temperature. As the temperature increases, the microhardness of the Co-Mo coating increases first and then decreases.

When the temperature is 40℃, 45℃, 55℃ and 60℃, the microhardness of Co-Mo coating are 320HV, 314HV, 397HV and 376HV. When the temperature is 50℃, the microhardness of the Co-Mo coating reaches the maximum value of 503HV. As the temperature increases, the content of molybdenum in the coating first increases and then decreases. The thickness of the coating also increases first and then decreases. Therefore, the microhardness of the coating first increases and then decreases.

3.1.5 Characterization of coating surface elements

XPS was used to test the composition and chemical valence state of the Co-Mo coating. XPS pattern of (a) full spectrum of elements, (b) Co2p, (c) O1s and (d) Mo3d of Co-Mo coating is shown in Fig. 13. As shown in Fig. 13 (a), the peaks of O, Co and Mo appear in the spectrum. As shown in Fig. 13 (b), the Co 2p1/2 XPS has two split peaks, belonging to Co (799.3 eV), Cobalt Oxides (804.1 eV). The Co 2p3/2 XPS has two split peaks, belonging to Co (779.1 eV), Cobalt Oxides (781.7 eV). Coating surface formed an oxide film when exposed to air. As shown in Fig. 8 (c), the O 1s XPS has one split peaks at 532.3 eV, which is related to the Er_2O_3 and the metal oxide. As shown in Fig. 8 (d), the Mo 3d XPS has three split peaks, belonging to Mo^{6+} (235.5 eV), Mo^{3+} (228.9 eV and 232.3 eV). The existence of Mo^{6+} is due to the oxidation of Mo to MoO_3 and the existence of Mo^{3+} is due to the oxidation of Mo to Mo_2O_3.As shown in Fig. 14, it can be seen that the distribution of Co and Mo elements is very uniform. Figure 14(b) shows the EDS spectrum and the composition of the Co-Mo coating, the peaks of Co and Mo appear on the EDS pattern.

3.2 The electrochemical behavior of the deposition of Co-Mo alloy

3.2.1 Deposition potential

Figure 15(a) shows the cyclic voltammetry curves of cobalt-molybdenum plating solutions with different concentrations Na_2MoO_4 on glassy carbon electrodes. When the concentration of Na_2MoO_4 is 0.05 mol/L, 0.075mol/L, 0.1 mol/L, 0.125mol/L and 0.15 mol/L, the reduction peak appears at -0.85V, -0.9V, -0.95V, -1V and − 1.05V during the negative scan, and the oxidation peak appears at -0.25V, -0.3V,-0.33V and − 0.35V during the positive scan. Figure 15(b) shows the cyclic voltammetry curves of cobalt-molybdenum plating solutions with different concentration of $C_6H_5Na_3O_7$ on glassy carbon electrodes. When the concentration of $C_6H_5Na_3O_7$ is 0.1 mol/L, 0.15 mol/L, 0.2mol/L, 0.25mol/L and 0.3mol/L, the reduction peak appears at -0.85V, -0.75V, -0.9V, -0.95V and − 1V during the negative scan, and the oxidation peak appears at -0.25V, -0.1V, -0.3V, -0.35V and − 0.38V during the positive scan. Figure 15(c) shows the cyclic voltammetry curves of cobalt-molybdenum baths with different pH on glassy carbon electrodes. When the pH is 5, 6, 7 and 8, the reduction peak appears at -0.75V, -0.8V, -0.9V and − 1V when scanning in the negative direction, and the oxidation peak appears at -0.15V, -0.25V, -0.3V and − 0.35V

when scanning in the forward direction. When the pH is 9, there is almost no redox peak. Figure 15(d) shows the cyclic voltammetry curves of cobalt-molybdenum baths with different temperature on glassy carbon electrodes. When the temperature is 40℃, 45℃, 50℃, 55℃ and 60℃, the reduction peak appears at -0.89V, -0.87V, -0.85V, -0.84V and − 0.82V when scanning in the negative direction, and the oxidation peak appears at -0.25V, -0.26V, -0.27V, -0.29V and − 0.32V when scanning in the forward direction.

It can be seen from the CV graph that as the concentration of Na_2MoO_4 increases, the deposition potential of the cobalt-molybdenum alloy moves in a negative direction. The reason for this trend is that when the concentration of Na_2MoO_4 increases, too much molybdate ions make the migration rate of complex ions slow, and the precipitation potential shifts in the negative direction; as the concentration of $C_6H_5Na_3O_7$ increases, the deposition potential of the cobalt-molybdenum alloy first shifts to a positive direction and then to a negative direction. The reason for this trend is that when the concentration of $C_6H_5Na_3O_7$ increases, the number of cobalt-molybdenum complex ions formed increases, which facilitates the deposition of cobalt-molybdenum complex ions, thereby shifting the precipitation potential to the positive direction. When the concentration of $C_6H_5Na_3O_7$ is high, the ionization equilibrium is destroyed, resulting in the pH of the plating solution; as the pH increases, the deposition potential of the cobalt-molybdenum alloy shifts in the negative direction. The reason for this trend is that when the pH value is high, Co(Ⅱ) exists in the form of $CoCit^-$, and molybdenum exists in the form of MoO_4^{2-}; when the pH value is low, Co(Ⅱ) exists in the form of HCoCit, molybdenum exists in the form of HrMoO4Cit[5–r] [11]; as the temperature rises, the deposition potential of the cobalt-molybdenum alloy shifts in the positive direction. This is because as the temperature rises, the migration rate of ions increases, and the stability of complex ions is destroyed, so it is more conducive to the deposition of cobalt, and the deposition potential moves forward.

3.2.2 Exchange current density

The exchange current density is an important kinetic parameter to evaluate the electrode reaction: The higher the exchange current density, the easier the electrode reaction. Therefore, the exchange current density i_0 on the glassy carbon electrode in the bath was studied by LSV. The Butler-Volmer[23, 24] equation was applied at very low cathode overpotential, which can be simplified to Eq. (2), Take the logarithm of both sides of Eq. (2) to obtain Eq. (3).

$$i = i_0\left\{ - exp\left[\frac{-\alpha nF}{RT}\eta\right]\right\}$$

2

$$\log|i| = \log\left|i_0\right| - \frac{\alpha nF}{RT}\eta$$

3

where i is the current density ($mA \cdot cm^{-2}$), i_0 is the exchange current density ($mA \cdot cm^{-2}$), α is the charge transfer coefficient in the cathode direction, η is over-potential.

Based on the Eq. (3), it can be found that under a small overpotential, i and η are linearly related. When the overpotential exceeds − 0.1 V, the current contribution of anode polarization is negligible. Therefore, the value of i_0 can be measured by the slope of the i-η curve in a narrow potential range close to the equilibrium potential.

Figure 16 shows the LSV curve on glassy carbon electrode in the bath, where when η is between − 0.15 V and − 0.1 V, the polarization curve presents a straight line.

Table 2 shows the value of exchange current density i_0 on glassy carbon electrode in the bath, it can be found that as the concentration of Na_2MoO_4 increases, the exchange current density i_0 decreases; as the concentration of $C_6H_5Na_3O_7$ increases, the exchange current density i_0 increases first and decreases then, when the concentration of $C_6H_5Na_3O_7$ is 0.05mol/L, i_0 reaches a maximum; as the pH increases, the exchange current density i_0 decreases; as the temperature increases, the exchange current density i_0 increases.

Table 2
The value of exchange current density i_0 on glassy carbon electrode in the bath

$C_{Na2MoO4}$ (mol/L)	i_0 ($mA \cdot cm^{-2}$)	$C_{C6H5Na3O7}$(mol/L)	i_0	pH	i_0	Temperature (℃)	i_0
0.05	0.0703	0.1	0.0661	5	0.1296	40	0.1975
0.075	0.0702	0.15	0.0703	6	0.0703	45	0.2306
0.1	0.0687	0.2	0.0523	7	0.0458	50	0.2413
0.125	0.0534	0.25	0.0313	8	0.0314	55	0.2452
0.15	0.0385	0.3	0.0150	9	0.0158	60	0.2458

3.2.3 Charge transfer impedance

Figure 17 shows Nyquist plots at -1.2 V potential in the bath. It is observed that there is only one EIS spectrum composed of a semicircular arc, which indicates that the deposition of alloy is only controlled by charge transfer[25].

According to the impedance results, Zview software was used to fit the equivalent circuit, and the result is shown as Fig. 17(e). In the circuit, *Rs* is the resistance of the solution, *Rct* is the charge transfer resistance, CPE is a constant phase element used to establish a more accurate fit.

As shown in Table 3, as the concentration of Na_2MoO_4 increases, the charge transfer resistance *Rct* increases; as the concentration of $C_6H_5Na_3O_7$ increases, the charge transfer resistance *Rct* decreases first and then increases; as the pH increases, the charge transfer resistance *Rct* increase; as the temperature increases, the charge transfer resistance *Rct* decreases.

Table 3
The value of *Rs* and *Rct* on copper electrode in the bath

$C_{Na2MoO4}$ (mol/L)	Rct (ohms·cm^2)	$C_{C6H5Na3O7}$ (mol/L)	Rct	pH	Rct	temperature	Rct
0.05	13.9000	0.1	15.4158	5	11.0002	40℃	9.6225
0.075	20.5874	0.15	13.9000	6	13.9000	45℃	8.5698
0.1	23.9291	0.2	16.7228	7	14.2071	50℃	8.4991
0.125	30.9588	0.25	16.8429	8	15.4511	55℃	8.3437
0.15	47.9219	0.3	19.2591	9	30.5490	60℃	8.0187

4. Conclusion

In this paper, Co-Mo coating was prepared on the copper substrate by electrodeposition. The influence of different process parameters on the kinetics of deposition of alloy and structure, morphology, composition and mechanical properties of coating was studied. The conclusions are as follows:

By studying the effects of different factors on the structure, composition, morphology and properties of the coating, it is determined that the optimum process conditions for electrodeposition of Co-Mo coating are as follows: the concentration of Na_2MoO_4 is 0.05mol/L, the concentration of $C_6H_5Na_3O_7$ is 0.15mol/L, the pH of the plating solution is 7 and the temperature is 50℃. Under these conditions, the coating is an amorphous alloy with dense nodular morphology, the content of Mo is 39.56% and the microhardness is 503HV.

Through the study of electrodeposition behavior of Co-Mo alloy under different factors, it is found that smaller concentration of Na_2MoO_4, appropriate concentration of $C_6H_5Na_3O_7$, smaller plating solution pH and higher temperature made the reduction potential move forward, the exchange current increase and the charge transfer impedance decrease.

Declarations

Acknowledgements

This work was supported by National Key R&D Program of China (2018YFC1901700), National Natural Science Foundation of China (52025042, 51621003).

Author contribution statements

Ya Tian wrote the main manuscript text, Liwen Ma and Xiaoli Xi revised the language ,overall structure of the manuscript and provided research funding, and Zuoren Nie provided research funding.

Data Availability Statement

The data used to support the findings of this study are included within the article.

Declaration of interests

The authors declare that they have no known competing financial interests or personal relationships that could have appeared to influence the work reported in this paper.

References

1. Elias L.& Chitharanjan A. H. A comparative study on the electrocatalytic activity of electrodeposited Ni-W and Ni-P alloy coatings. Mater today: proceedings 5, 21156–21161(2018). https://doi.org/10.1016/j.matpr.2018.06.514.
2. Argañaraz M. P. Q., et al. The chemistry and structure of nickel–tungsten coatings obtained by pulse galvanostatic electrodeposition. Electrochim. Acta 72, 87–93 (2012). https://doi.org/10.1016/j.electacta.2012.03.163.
3. Vernickaite E., Tsyntsaru N. & Cesiulis H. Electrodeposited Co-W alloys and their prospects as effective anode for methanol oxidation in acidic media. Surf. Coat. Tech. 307,1322–1328(2016). https://doi.org/10.1016/j.surfcoat.2016.07.049.
4. Vernickaite E., Tsyntsaru N., Sobczak K. & Cesiulis H. Electrodeposited tungsten-rich Ni-W, Co-W and Fe-W cathodes for efficient hydrogen evolution in alkaline medium. Electrochim. Acta 318, 597–606(2019). https://doi.org/10.1016/j.surfcoat.2016.07.049.
5. Tsyntsaru N., et al. Toward uniform electrodeposition of magnetic Co-W mesowires arrays: direct versus pulse current deposition. Electrochim. Acta 188,589–601(2016). https://doi.org/10.1016/j.electacta.2015.12.032.
6. Stepanova L. I. & Purovskaya O. G., Electrodeposition of Nickel-Based alloys with tungsten and molybdenum. Met. Finish. 96, 50, 50–52, 53 (1998). https://doi.org/10.1016/S0026-0576(98)80871-4.
7. Ashraf M. A., Liu Z., Pham B. T. & Zhang D. Electrodeposition of superhydrophilic and binder-free Mo-doped Ni-Fe nanosheets as cost-effective and efficient bifunctional electrocatalyst for overall water

splitting. J. Electroanal. Chem. 873,114351(2020). https://doi.org/10.1016/j.jelechem.2020.114351.

8. Wasekar N. P., Verulkar S. & Vamsi M. V. N., Sundararajan G. Influence of molybdenum on the mechanical properties, electrochemical corrosion and wear behavior of electrodeposited Ni-Mo alloy. Surf. Coat. Tech. 370,298–310(2019). https://doi.org/10.1016/j.surfcoat.2019.04.059.
9. Evariste U., Jiang G., Yu B., Liu Y. & Ma P. One-step electrodeposition of molybdenum nickel cobalt sulfides on ni foam for high-performance asymmetric supercapacitors. J. Energy Storage 29,101419(2020). https://doi.org/10.1016/j.est.2020.101419.
10. Yar-Mukhamedova G., Ved'M., Sakhnenko N. & Nenastina T. Electrodeposition and properties of binary and ternary cobalt alloys with molybdenum and tungsten. Appl. Surf. Sci. 445,298–307(2018). https://doi.org/10.1016/j.apsusc.2018.03.171.
11. Gómez E., Pellicer E. & Vallés E. Influence of the bath composition and the pH on the induced cobalt-molybdenum electrodeposition. J. Electroanal. Chem. 556,137–145(2003). https://doi.org/10.1016/S0022-0728(03)00339-5.
12. Gómez E., Pellicer E. & Vallés E. Microstructures of soft-magnetic cobalt-molybdenum alloy obtained by electrodeposition on seed layer/silicon substrates. Electrochem. Commun. 6,853–859(2004). https://doi.org/10.1016/j.elecom.2004.06.011.
13. Aaboubi O. & Msellak K., Magnetic field effects on the electrodeposition of CoNiMo alloys. Appl. Surf. Sci. 396, 375–383(2017). https://doi.org/10.1016/j.apsusc.2016.10.164.
14. Costa J. M., Hori M. S. & de Almeida Neto A. F. Effects of the forced convection and current density on the electrodeposition of Zn-Fe-Mo alloys. Chem. Phys. 527:110502 (2019). https://doi.org/10.1016/j.chemphys.2019.110502.
15. Winiarski J., Tylus W., Krawczyk M. S. & Szczygieł B. (2016) The influence of molybdenum on the electrodeposition and properties of ternary Zn-Fe-Mo alloy. coatings.Electrochim. Acta 196,708–726(2016). https://doi.org/10.1016/j.electacta.2016.03.027
16. Hara A., Świątek Z. & Ozga P. The role of surfactants in induced electrodeposition of Zn–Mo layer from citrate solutions. J. Alloy. Compd. 827,154195(2020). https://doi.org/10.1016/j.jallcom.2020.154195.
17. Z. Lian, et al. Electrodeposition of tungsten coatings on molybdenum substrates and deuterium irradiation effect. Fusion Eng. Des. 112,136–142(2016). https://doi.org/10.1016/j.fusengdes.2016.08.003.
18. Li C., Bo X., Li M. & Guo L. Facile electrodeposition fabrication of molybdenum-tungsten sulfide on carbon cloth for electrocatalytic hydrogen evolution. Int. J. Hydrogen Energ. 42,15479–15488(2017). https://doi.org/10.1016/j.ijhydene.2017.05.046.
19. Jiang F., Xue J., Chen Y. & Zhang Y. Effect of heat treatment on physical properties of tungsten coating obtained by pulse electrodeposition. Fusion Eng. Des. 150,111332(2020). https://doi.org/10.1016/j.fusengdes.2019.111332.
20. Zhu T., Chong M. N., Phuan Y. W., Ocon J.D. & Chan E.S. Effects of electrodeposition synthesis parameters on the photoactivity of nanostructured tungsten trioxide thin films: Optimisation study

using response surface methodology. J. Taiwan Inst. Chem. E. 61,196–204(2016). https://doi.org/10.1016/j.jtice.2015.12.010.

21. Lee C. Y., Mao W. T., Ger M. D., Lee H. B. A study on the corrosion and wear behavior of nanocrystalline Ni-Mo electrodeposited coatings. Surf. Coat. Tech. 366,286–295(2019). https://doi.org/10.1016/j.surfcoat.2019.03.048
22. Beltowska-Lehman E. & Indyka P. Kinetics of Ni-Mo electrodeposition from Ni-rich citrate baths. Thin Solid Films 520,2046–2051(2012). https://doi.org/10.1016/j.tsf.2011.10.024.
23. Guo S., Wu E. & Zhang J. Exchange current density of Gd(III)/Gd reaction in LiCl-KCl eutectic and analysis of errors caused by various methods. Electrochim. Acta 259,253–261(2018). https://doi.org/10.1016/j.electacta.2017.10.158.
24. Lim K. H. & Yun J. Study on the exchange current density of lanthanide chlorides in LiCl-KCl molten salt. Electrochim. Acta 295,577–583(2019). https://doi.org/10.1016/j.electacta.2018.10.104.
25. Yoon D. & Phongikaroon S. Measurement and Analysis of Exchange Current Density for U/U3 + Reaction in LiCl-KCl Eutectic Salt via Various Electrochemical Techniques. Electrochim. Acta 227,170–179(2017). https://doi.org/10.1016/j.electacta.2017.01.011.

Figures

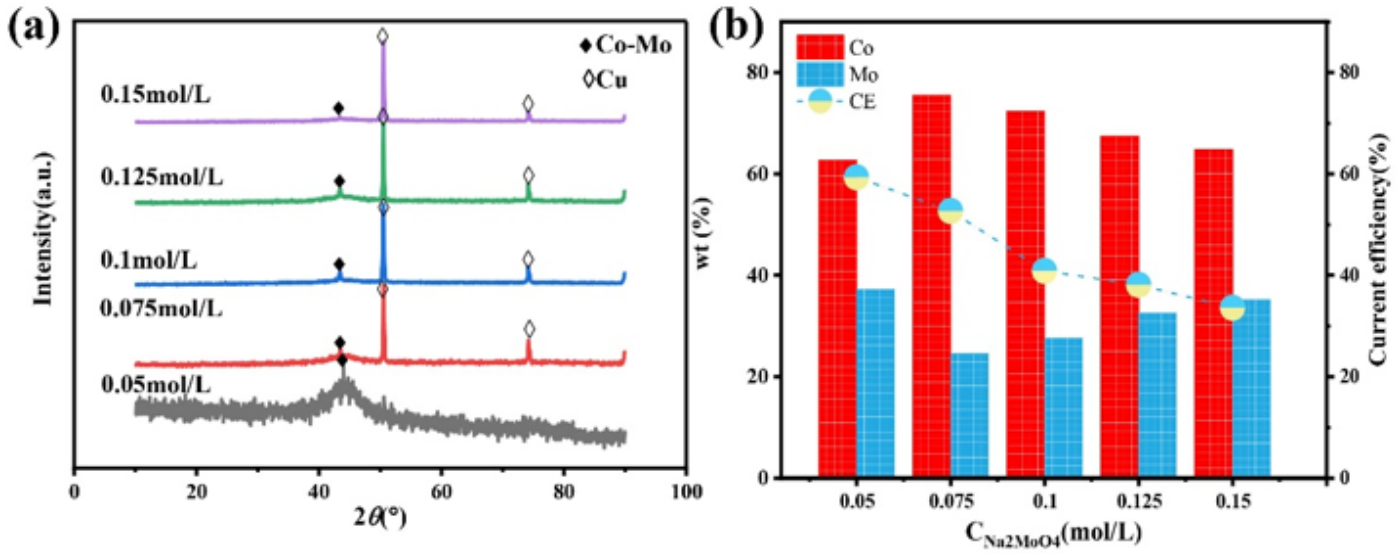

Figure 1

(a) XRD of Co-Mo coatings under different concentrations of Na_2MoO_4;(b) The effect of the concentration of Na_2MoO_4 on the composition and current efficiency of the Co-Mo coating

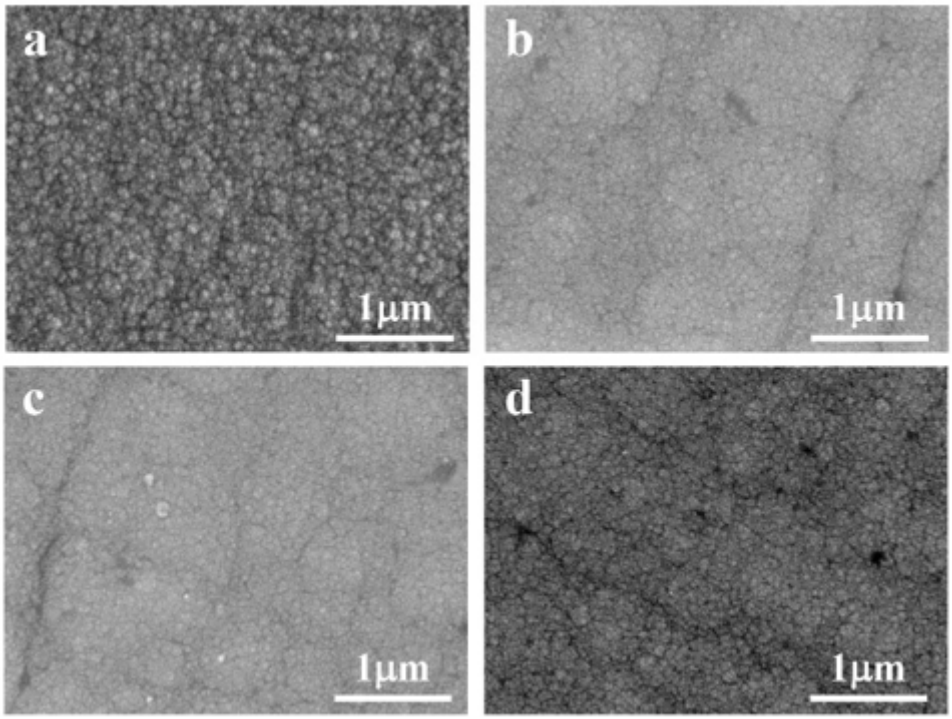

Figure 2

SEM of Co-Mo coatings under different concentrations of Na_2MoO_4 (a) 0.05 mol/L; (b) 0.075 mol/L;(c) 0.1 mol/L;(d) 0.125 mol/L

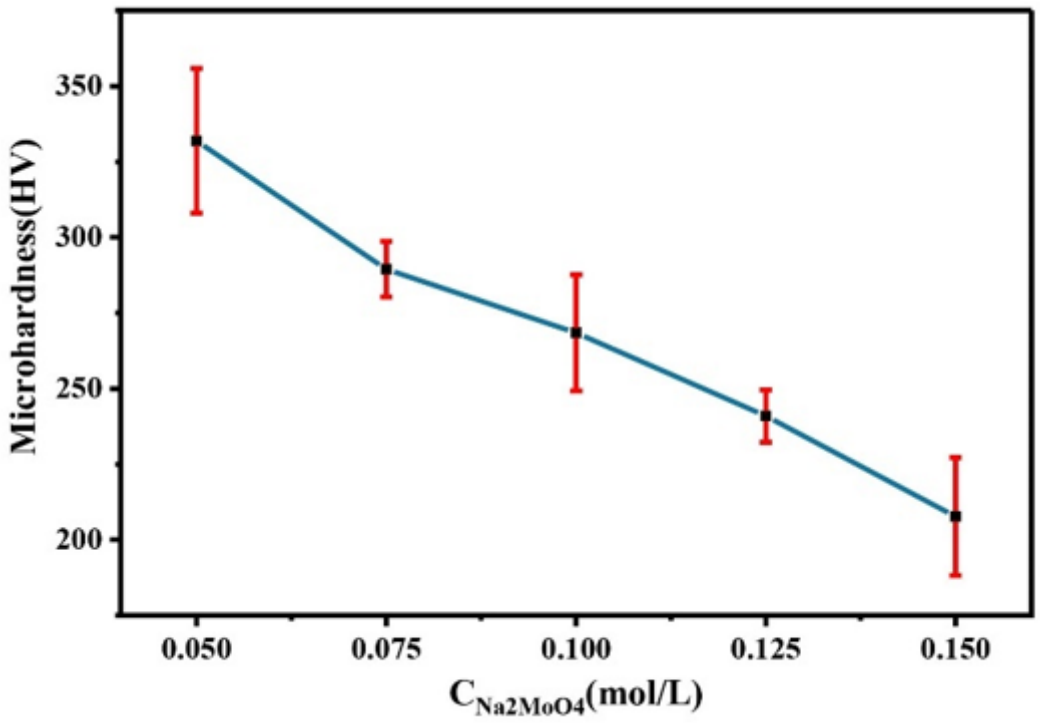

Figure 3

The microhardness of Co-Mo coatings with different concentrations of Na_2MoO_4

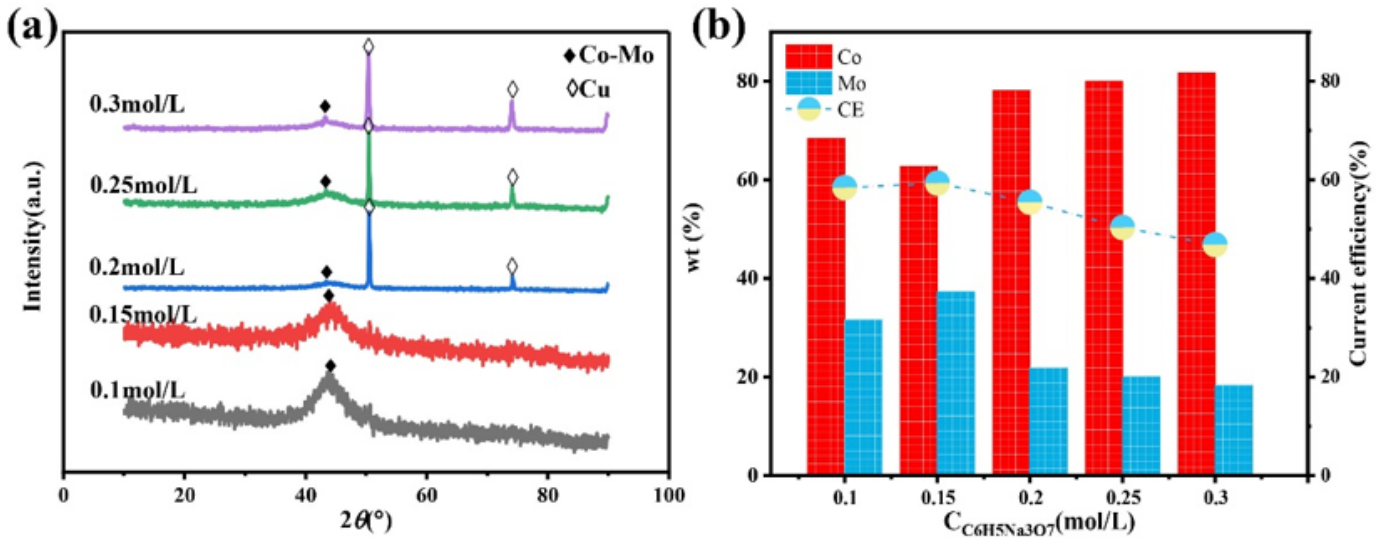

Figure 4

(a) XRD of Co-Mo coatings under different concentrations of $C_6H_5Na_3O_7$;(b) The effect of the concentration of $C_6H_5Na_3O_7$ on the composition and current efficiency of the Co-Mo coatings

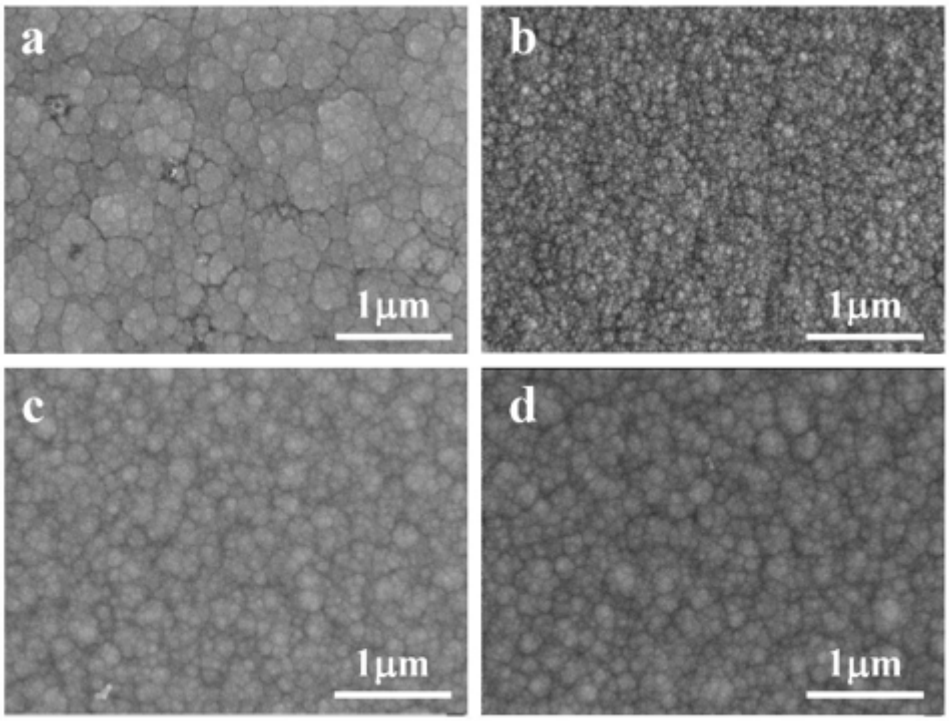

Figure 5

SEM of Co-Mo coatings under different concentrations of $C_6H_5Na_3O_7$ (a) 0.1 mol/L; (b) 0.15mol/L;(c) 0.2mol/L;(d) 0.25mol/L

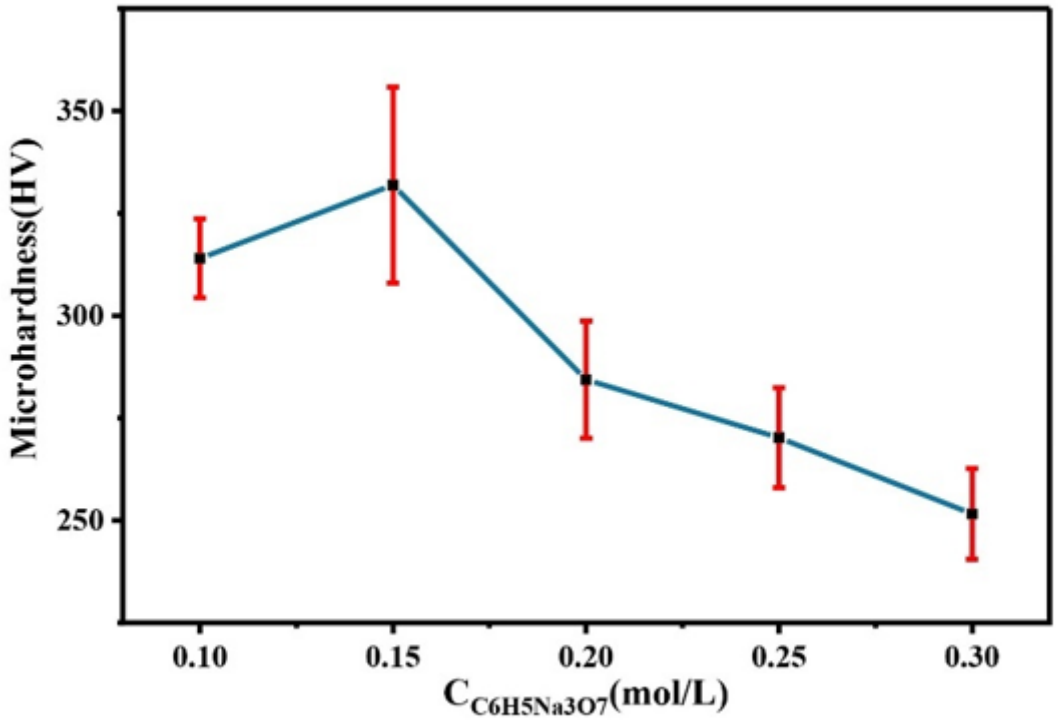

Figure 6

The microhardness of Co-Mo coatings with different concentrations of $C_6H_5Na_3O_7$

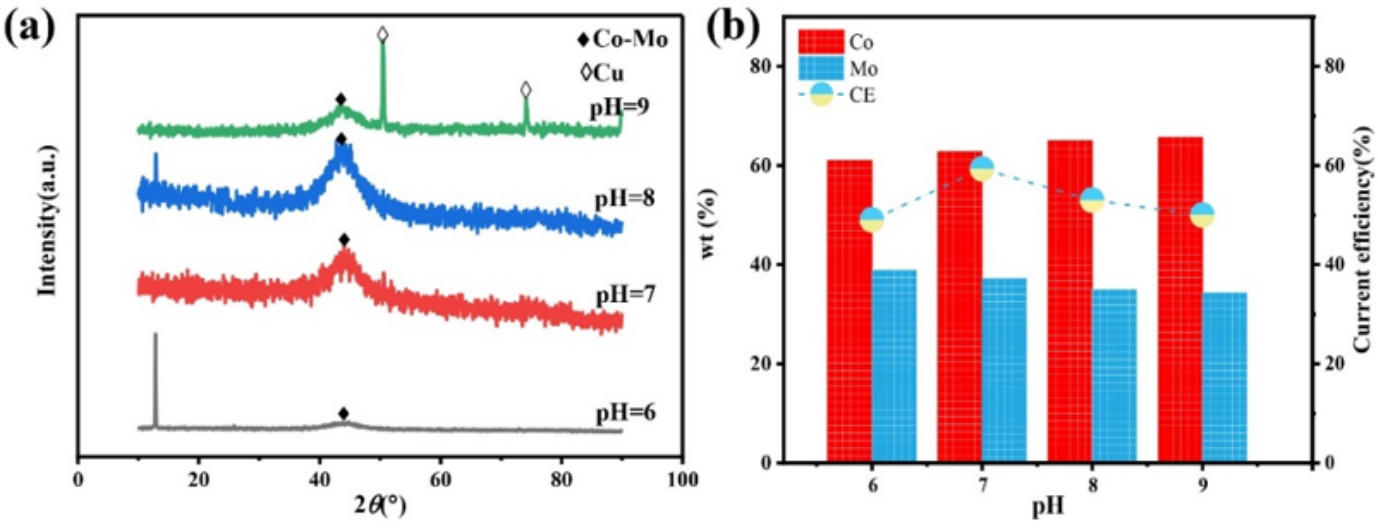

Figure 7

(a) XRD of Co-Mo coatings under different pH;(b) The effect of pH on the composition and current efficiency of the Co-Mo coatings

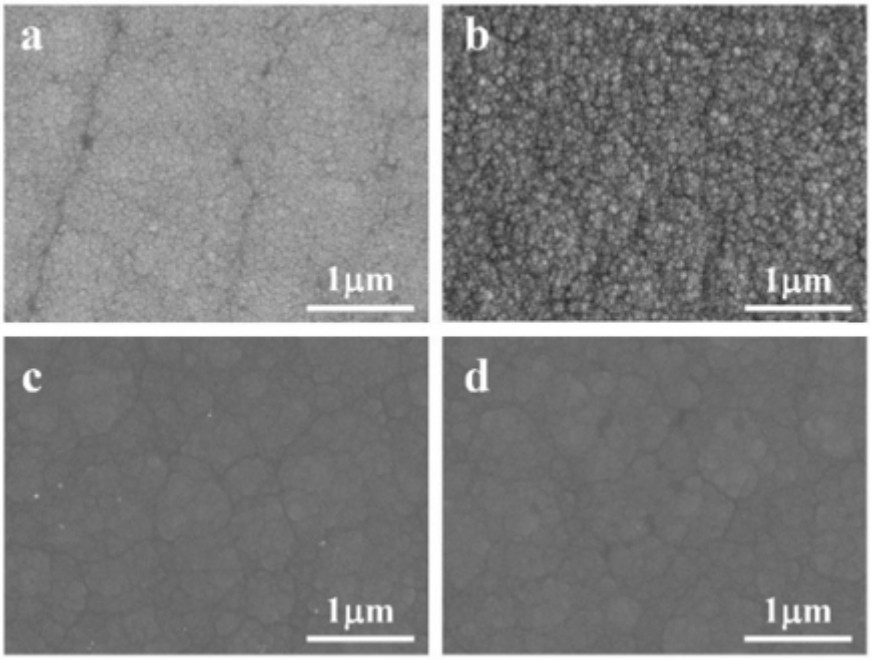

Figure 8

SEM of Co-Mo coatings under different pH (a) pH=6; (b) pH=7;(c) pH=8;(d) pH=9

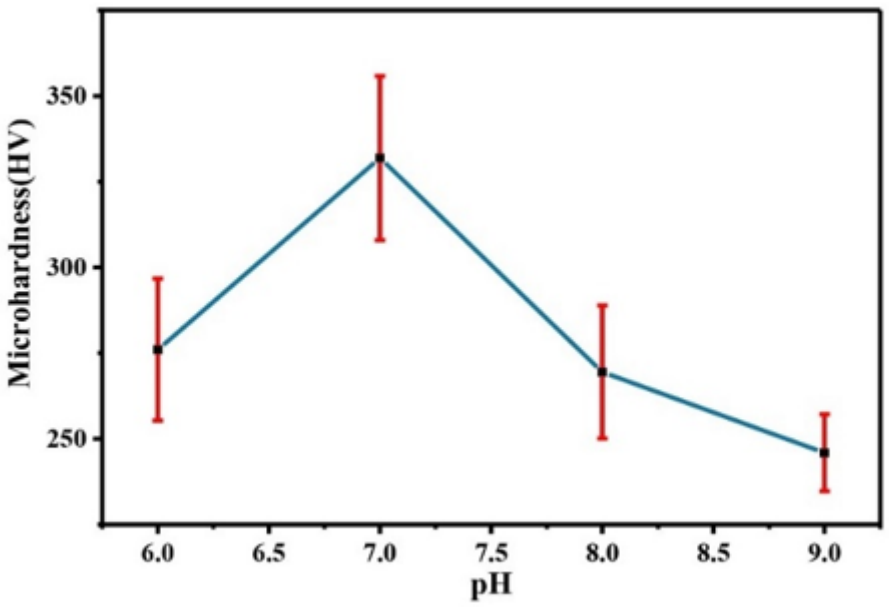

Figure 9

The microhardness of Co-Mo coatings under different pH

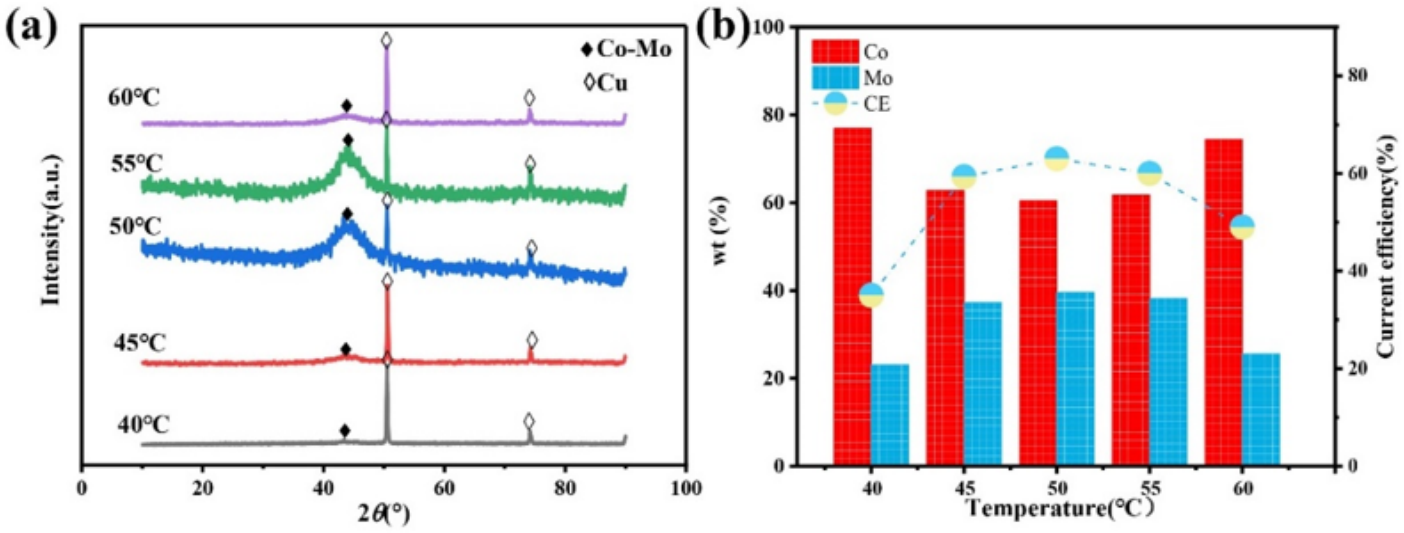

Figure 10

(a) XRD of Co-Mo coatings under different temperature;(b) The effect of temperature on the composition and current efficiency of the Co-Mo coatings

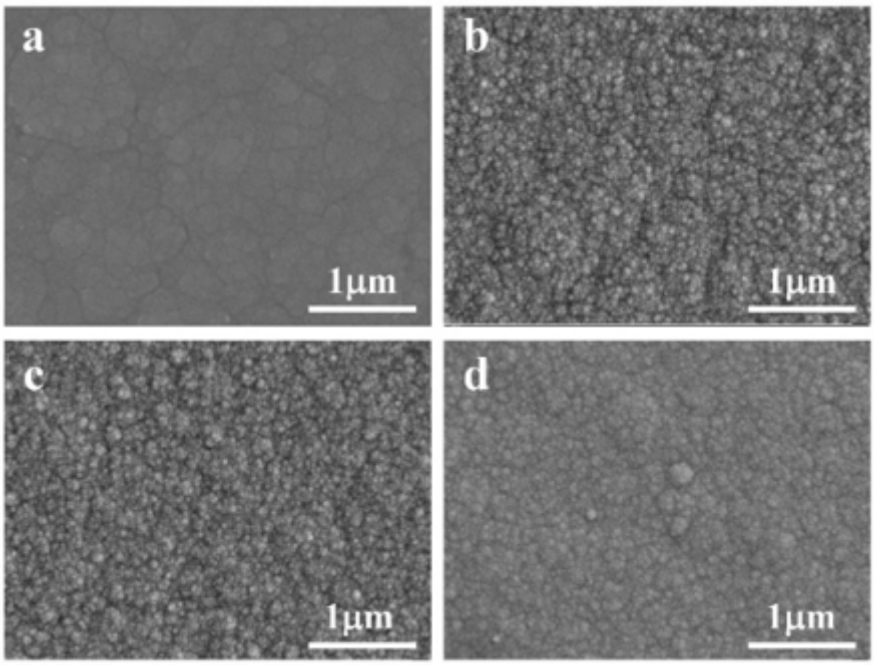

Figure 11

SEM of Co-Mo coatings under different temperature (a) 40°C; (b) 45°C;(c) 50°C;(d) 55°C

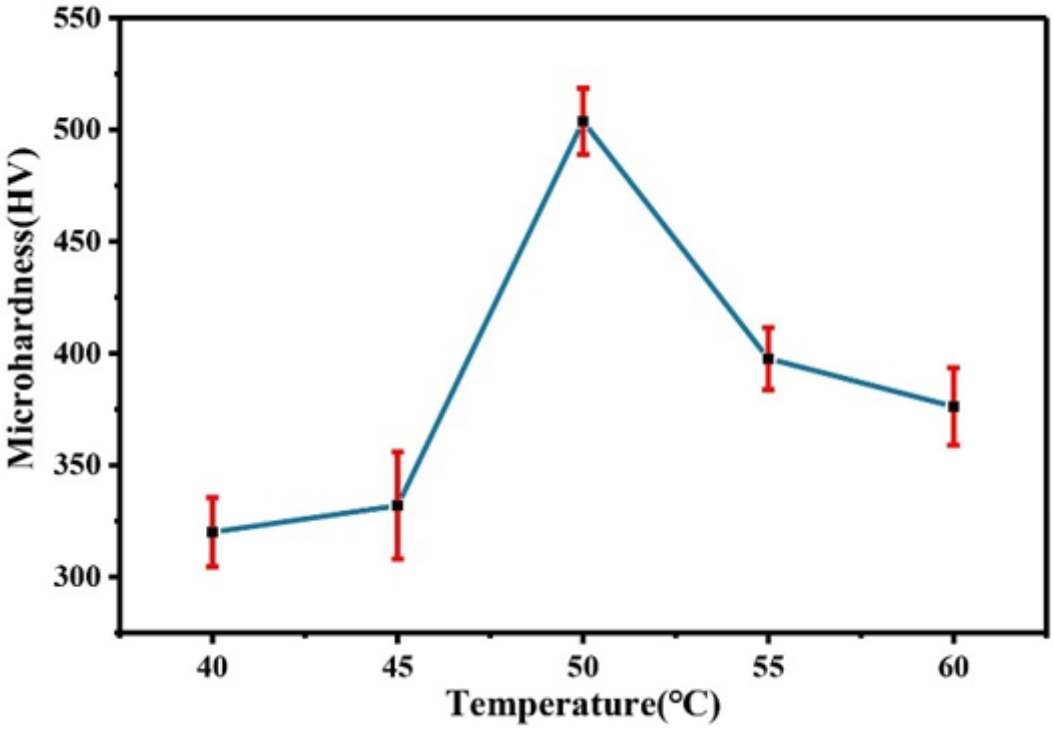

Figure 12

The microhardness of Co-Mo coatings under different temperature

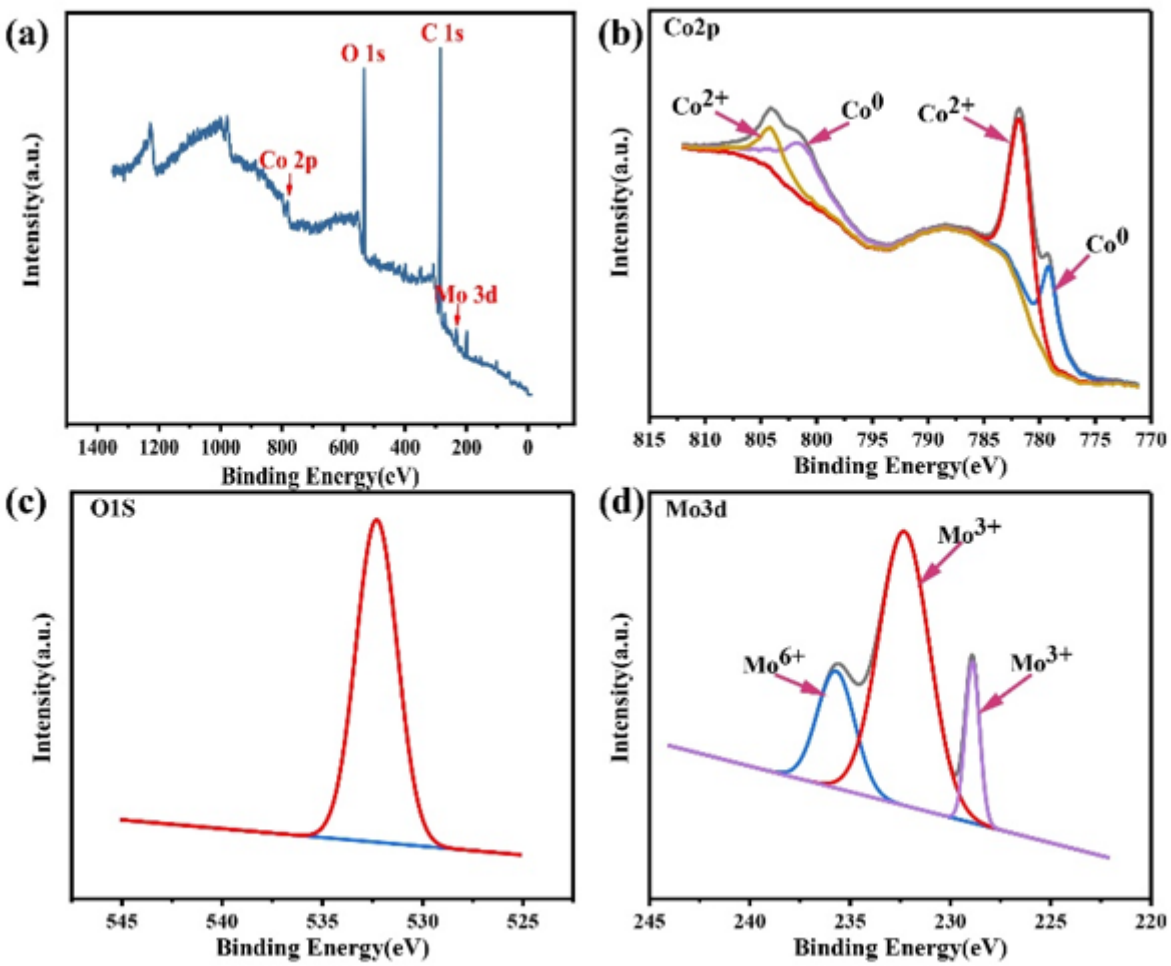

Figure 13

XPS spectra of Co-Mo coating (a)full spectrum of elements, (b) Co2p, (c) O1s, (d) Mo3d

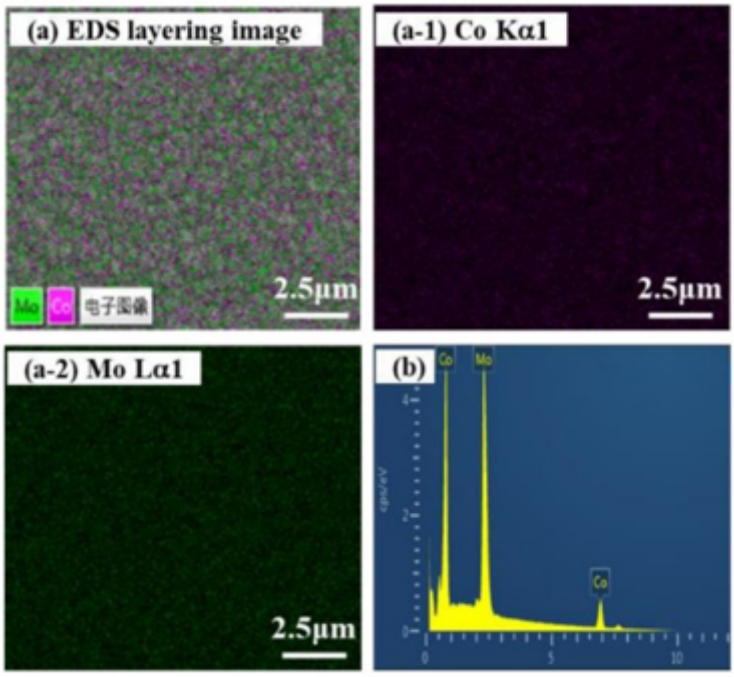

Figure 14

SEM (a), element distribution (a-1)-(a-2) and EDS spectrum (b) of Co-Mo coating

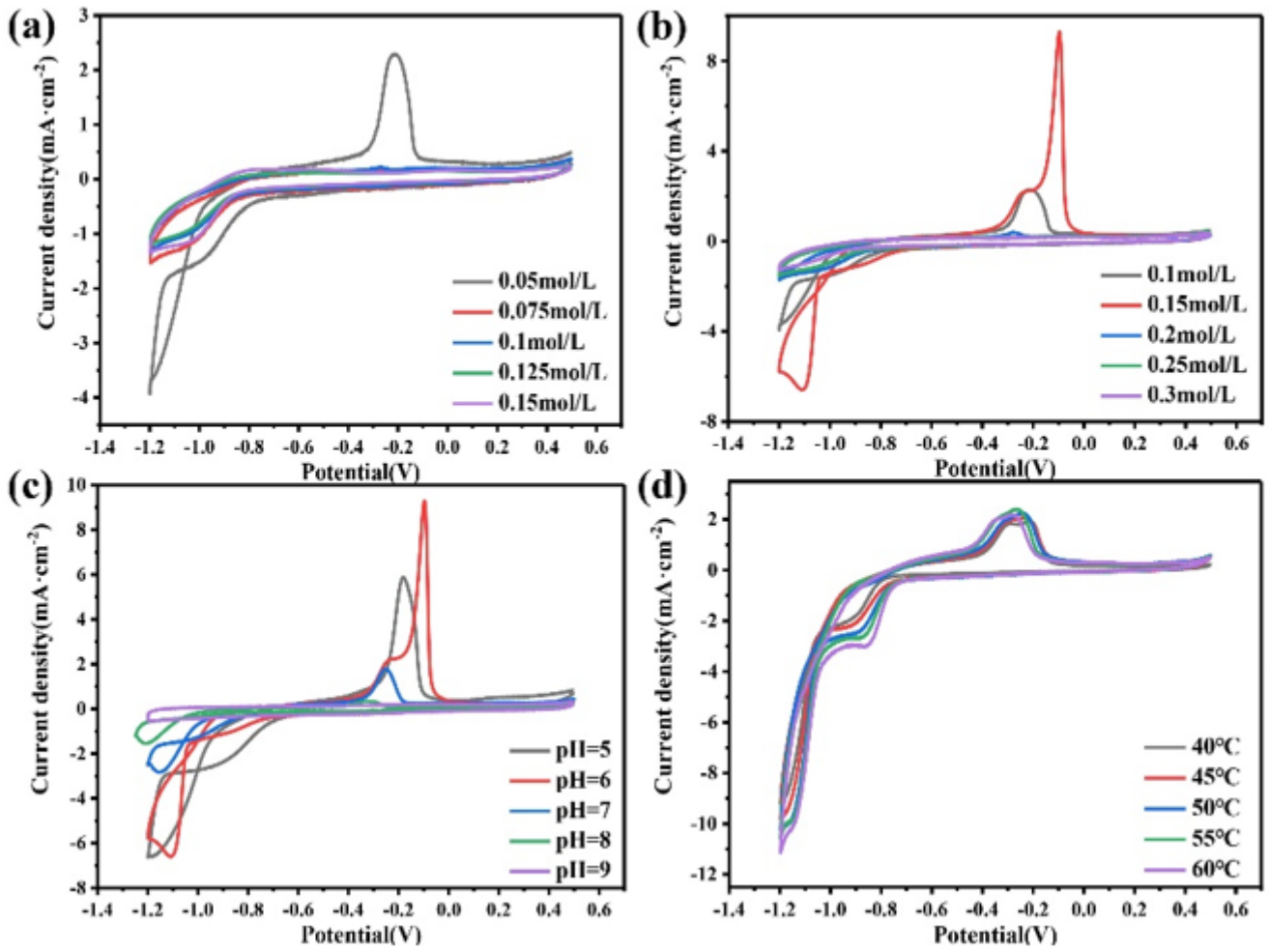

Figure 15

CV curves obtained on glassy carbon electrode in the bath with different(a) concentration of Na_2MoO_4 ; (b) concentration of $C_6H_5Na_3O_7$;(c) pH;(d) temperature

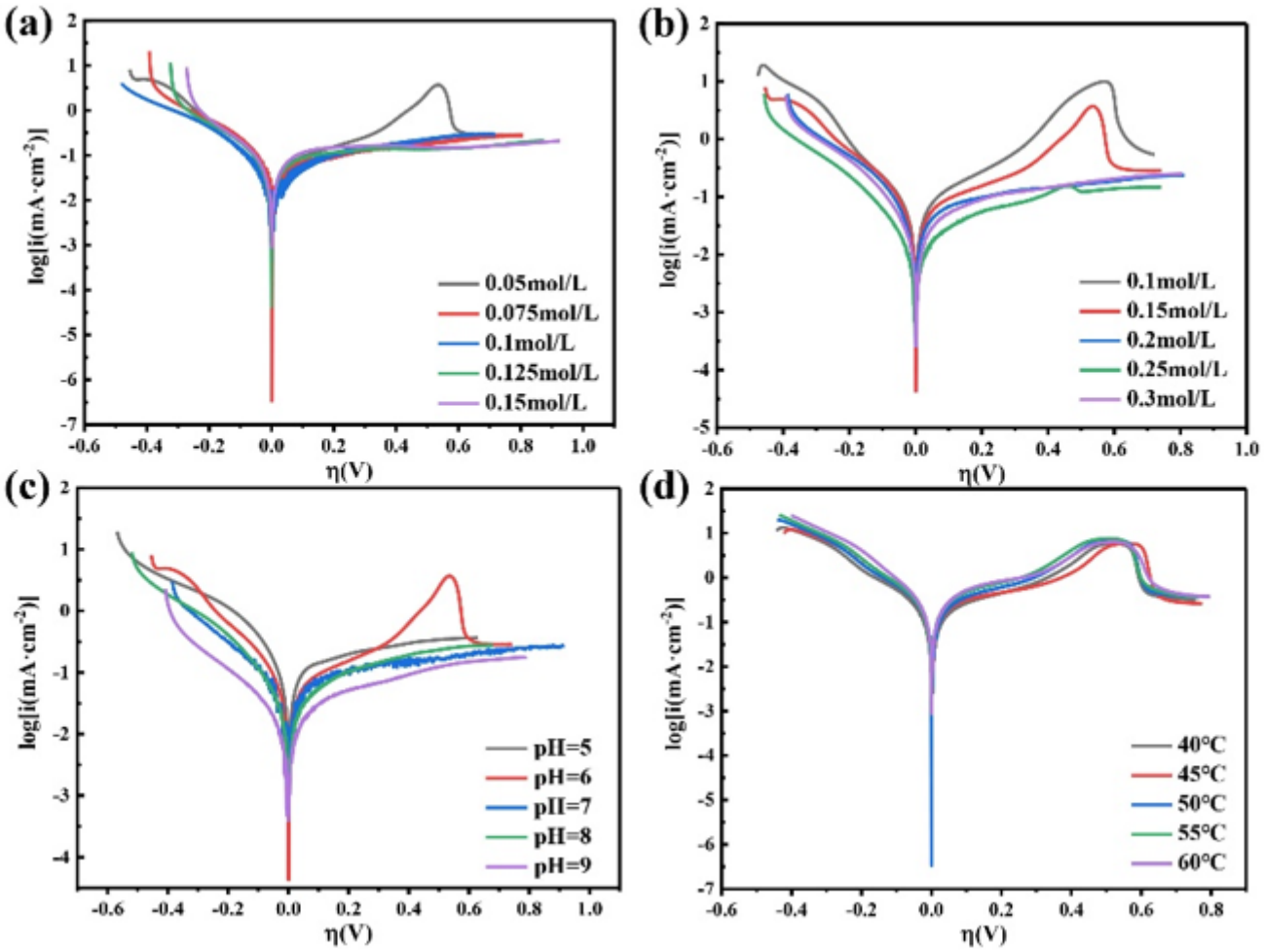

Figure 16

LSV curves obtained on glassy carbon electrode in the bath with different(a) concentration of Na_2MoO_4 ; (b) concentration of $C_6H_5Na_3O_7$;(c) pH;(d) temperature

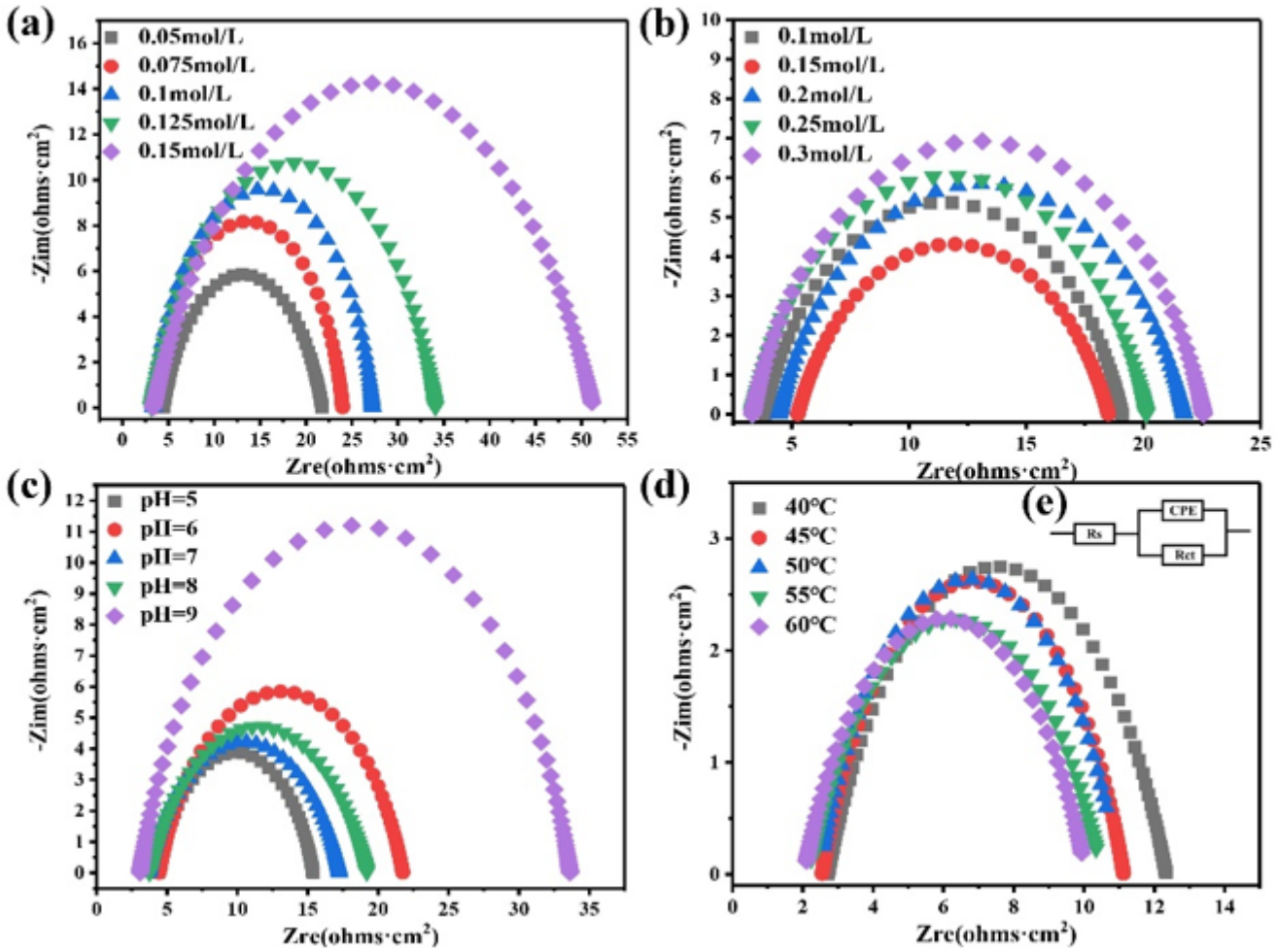

Figure 17

Nyquist plots at -1.2 V potential in the bath with different (a) concentration of Na_2MoO_4 ;(b) concentration of $C_6H_5Na_3O_7$;(c) pH;(d) temperature;(e) equivalent circuit